Proudman Oceanographic Laboratory
NATURAL ENVIRONMENT RESEARCH COUNCIL

A three dimensional finite element model of wind effects upon higher harmonics of the internal tide.

P. Hall *, A.M. Davies
Proudman Oceanographic Laboratory, 6 Brownlow Street, Liverpool L3 5DA, UK.

Abstract

A non–linear three dimensional unstructured grid model of the M_2 tide in the shelf edge area off the west coast of Scotland is used to examine the spatial distribution of the M_2 internal tide and its higher harmonics in the region. In addition the spatial variability of the tidally induced turbulent kinetic energy and associated mixing in the area are considered. Initial calculations involve only tidal forcing, although subsequent calculations are performed with up–welling and down–welling favourable winds in order to examine how these influence the tidal distribution (particularly the higher harmonics) and mixing in the region. Both short and long duration winds are used in these calculations. Tidal calculations show that there is significant small scale spatial variability particularly in the higher harmonics of the internal tide in the region. In addition turbulence energy and mixing exhibit appreciable spatial variability in regions of rapidly changing topography, with increased mixing occurring above seamounts. Wind effects significantly change the distribution of the M_2 internal tide and its higher harmonics, with appreciable differences found between up– and down–welling winds, and long and short duration winds due to differences in mixing and the presence of wind induced flows. The implications for model validation, particularly in terms of energy transfer to higher harmonics, and mixing are briefly discussed.

1. INTRODUCTION

Over the last thirty years there has been significant progress in computing tidal elevations and current profiles in shallow sea regions under homogeneous conditions. Initial calculations were two dimensional and used coarse finite difference grids which could not resolve near coastal regions. Consequently the main focus was on the M_2 tide (Flather, 1976), rather than its higher harmonics that were produced by non–linear effects in shallow coastal regions. With advances in computing power, finite difference grids were refined and three dimensional models developed to examine current structure (Davies and Kwong, 2000). Although finite difference grids became progressively finer, the majority of calculations were based on a uniform grid and hence resolution in nearshore regions was limited. To avoid this problem boundary fitted coordinates were developed in order to improve resolution in nearshore regions.

An alternative approach to the finite difference method was to use finite elements (e.g. Walters and Werner (1989); Werner (1995); Walters (2005); Fortunato et al. (1997, 1999); Heniche et al. (2000); Ip et al. (1998); Jones and Davies (2006)). In these models the element size could be varied from coarse offshore to fine in nearshore regions. Consequently the generation of higher harmonics of the tide in nearshore regions could be accurately reproduced in large area models (Jones and Davies, 2007).

With increasing computing power three dimensional models have been developed, and horizontal finite difference grids refined. In shallow sea regions where tidal mixing is strong and the water column remains well mixed then stratification effects upon tidal turbulence are absent. Consequently although tidal currents over a region may have been collected at different times, the periodic nature of the tides means that in essence a synoptic data set can be produced. In stratified regions, in particular those adjacent to topography (e.g. Dogger Bank, Proctor and James 1996) where stratification changes, the determination of tidal currents and associated internal tides as the barotropic

* Corresponding author.
Email address: phh@pol.ac.uk (P. Hall).

tide propagates over steep topography is more complex, due to the time evolving nature of the stratification.

Early internal tidal models used primarily analytical approaches (Craig 1987; Sherwin and Taylor 1989, 1990) and were of cross–sectional form. Subsequently three dimensional models using uniform grids were developed (e.g. Cummins and Oey 1997) and used to examine the generation of the internal tide in a range of geographical locations. These models showed the importance of along shelf topography, off shelf sea mounts (Xing and Davies 1998, hereafter XD98, Xing and Davies 1999), and how the shape of sea mounts and ridges influenced internal tide propagation.

The uniform nature of the grid resolution in these models meant that the focus was the generation and propagation of the M_2 internal tide in three dimensions rather than a study of processes generating higher harmonics of the internal tide. Although recently a cross section high resolution finite difference grid model was used to examine the generation of higher harmonics of the tide in the proximity of sea mounts (Lamb, 2004).

So far the majority of internal tide calculations used uniform finite difference models, and considered the M_2 tide. However, the shallow sea applications of finite element models, clearly shows that this approach is ideal in a shelf edge environment where both enhanced resolution is required at the shelf edge and at offshore locations e.g. seamounts. Recently calculations of the M_2 internal tide have been performed using finite elements to examine its generation in shelf edge regions and the effect of element resolution e.g. Hall and Davies (2005a), (hereafter referenced as HD05a). This involved a comparison with a fine resolution (2.4 km across shelf and 4.6 km along shelf) finite difference internal tide model, (XD 98), and calculations with a range of finite element meshes to compute the internal tide off the west coast of Scotland. The region covered by the model, namely the Malin–Hebrides shelf, was identical to that used by XD98, as were water depths, the open boundary conditions and vertical stratification. By this means a rigorous comparison was possible and the influence of finite element resolution on the internal tide was assessed. A comparison with limited measurements was also possible. Although the main features of the internal tide computed with the finite difference and fine finite element model were comparable, it was evident that the intensity of the M_2 internal tide in its generation region and its subsequent propagation was improved by using the finer mesh grid.

In this paper the work presented in HD05a is extended to examine the spatial distribution of the shorter wavelength higher harmonics of the internal tide in the Malin–Hebrides shelf region. In addition, how these harmonics and stratification in the shelf edge region changes in response to wind forcing is considered. By using a range of wind conditions, some insight as to the role meteorology has in modifying the internal tidal signal in different regions can be determined. In addition the results presented in HD05a, are extended to examine the spatial variability of higher tidal harmonics, namely M_4 and M_6. As these are due to non–linear effects, they are a good guide as to how internal tidal models are representing these processes. However, their short wavelength and associated variability is a major challenge both in terms of grid resolution, and collecting high resolution synoptic data sets for model validation. The importance of mixing in the lateral boundary layers of the ocean has been shown to have important consequences for the computed circulation produced by large scale models (e.g. Samelson 1998; Spall 2001). Since mixing is related to the breaking of small scale waves, then the energy transfer from the M_2 tide to the shorter wave higher harmonics is important in this energy transfer to mixing. However, as the present model is hydrostatic with a spatial resolution of order kilometres, then mixing has to be parameterized using a turbulence closure scheme. Here Mellor and Yamada (see Blumberg and Mellor 1987 for detail) is used in the vertical and the scale selective filter of Smagorinsky (1963) in the horizontal. As shown in HD05a, as the finite element grid is reduced for a specified filter parameter C in the Smagorinsky formulation, a Gibbs type oscillation occurs in the boundary layer close to topography. To remove this the filter parameter C in the Smagorinsky formulation needs to be increased, thereby smoothing the boundary layer. In addition, the extent to which wind induced mixing in the lateral boundary layers influences internal tide generation, particularly the higher harmonics and how this diffuses away from the lateral oceanic boundaries is very important. However, in terms of wind forced motion in boundary layers, as shown by Hall and Davies (2005c) (hereafter HD05b) it is necessary to choose an appropriate value of C in the Smagorinsky form of sub–grid scale parameterization in order to adequately represent the wind forced boundary layer on a given grid. The need to use sub–grid scale parameterizations of mixing in these models, which impact upon boundary layer stability and thickness means that it is difficult to get a rigorous numerically converged solution in the sense that the internal tide converges as the grid scale is reduced due to the fact that the mixing changes in these boundary layers and hence the density field in the region where the internal tide is produced. For this reason the higher resolution grid and appropriate sub–grid scale mixing as used by HD05a, in a successful simulation of the internal tide is used throughout.

An alternative approach would be to use a full three dimensional non–hydrostatic model on a very fine grid of order 10 m, with minimum fixed constant diffusion coefficients, thereby avoiding the sub–grid parameterization problem. However, as shown by Berntsen et al. (2007) this does not guarantee convergence as the grid is refined unless a scale selective filter and sub–grid scale mixing parameterization are included. In addition such a calculation would be computationally prohibitive. These problems concerning model convergence and mixing parameterization suggest that detailed internal tide turbulence measurements are required in shelf edge regions. However, as shown later there

is significant spatial variability in these, both of which are affected by the wind, suggesting that large detailed synoptic measurements are required for model validation. To the authors knowledge this is the first time that the three dimensional distribution of higher harmonics of the internal tides, associated turbulence intensities and the influence of wind effects upon them has been presented in a shelf edge region.

The order of the paper is such that the region considered and model are discussed in the next section. Subsequent sections describe the three dimensional variability of the higher harmonics of the internal tide. The response to wind forcing and the resulting changes in tidal distribution are considered later in the paper. Major findings and implications for data collection to validate internal tidal models are summarized at the end.

2. THE GEOGRAPHICAL REGION AND INTERNAL TIDAL MODEL.

As the full three–dimensional equations and the turbulence closure model were presented in Xing and Davies 1997 (hereafter XD97), they will not be repeated here, where only the main features of the equations are discussed. The hydrostatic approximation is used in the model and density is derived from temperature using the equation of state given in XD98. The model is forced by the barotropic tide introduced through the open boundary (HD05a) and the internal tide is generated as isotherms are moved over the topography. The model is fully prognostic, with free surface elevation changing as the tide propagates on and off shelf. Vertical mixing of momentum and density are parameterized using vertical eddy viscosity and diffusivity coefficients computed using a turbulence energy closure, namely Mellor and Yamada sub–model (e.g. Blumberg and Mellor 1987). As the form of the turbulence model and similar models is given elsewhere (e.g. Luyten et al. 1996, XD98) it will not be repeated here. As shown in HD05b the Smagorinsky (1963) form of horizontal eddy viscosity used here is particularly good at preventing the development of numerical instabilities when wind forced internal waves are generated on an irregular grid. However, as discussed previously and shown in (HD05a,b) the filter parameter C in the Smagorinsky formulation of viscosity must be chosen in an appropriate manner to match grid resolution in boundary layers, and does influence the extent of these layers. The value and grid resolution used here is identical to HD05a, which yielded an accurate M_2 internal tide.

As the short term modification of the internal tide due to wind forcing, rather than its seasonal variation are examined here, there is no applied surface heat flux. A surface boundary condition on momentum and turbulence of wind stress origin as in XD97, is applied at the sea surface with a quadratic friction law as in XD98 at the seabed. Identical barotropic tidal forcing to that used in the finite difference model (XD98) and finite element model (HD05a) was applied. The model uses a sigma coordinate representation in the vertical and 40 levels were used in the calculations. Sigma levels were such that enhanced resolution in the near–bed and near surface region (as in XD98, HD05a) where the internal tide was largest, was used in all calculations.

The finite element model (Fig. 1) is identical to that used by HD05a. The domain covers a range of water depths from the order of 10 m close to the coast to the order of 3000 m in the ocean. Water depth changes rapidly at the shelf edge (approximately the 200 m contour), as it does along the edge of the Anton Dohrn Seamount and Hebrides Terrace Seamount. As shown in XD98 and HD05a, in these regions there is appreciable internal tide generation. Detailed studies using a range of unstructured grid approaches (HD05b, Hall and Davies 2005b) showed that it was necessary to have a fine grid adjacent to the topography in order to accurately reproduce wind forced internal waves generated in regions of topographic change. This was achieved using the finite element grid (Fig. 2) found by HD05a to accurately reproduce the tide. By using the same mesh in the present calculations a direct comparison with HD05a is possible, enabling the effect of the wind upon the M_2 tide to be determined.

Initial conditions corresponded to a state of rest with zero elevation and current, with the same temperature profile (Fig. 3) as used by XD97, applied everywhere. This profile was identical to that used in HD05a, enabling comparisons to be made with earlier calculations. Tidal barotropic forcing at the M_2 period was applied along the open boundary and as found in HD05a, after 6 tidal cycles a periodic barotropic tide and quasi–periodic baroclinic tide were established, which was harmonically analysed. Since boundary layer mixing occurred in the model and modified the density field through time, this had the effect of slightly changing the baroclinic tide with time. Hence only a quasi–baroclinic tide was established. As HD05a, did not examine the higher harmonics of the tide, in an initial calculation (Calc. 1, Table 1) these are computed in a tide only solution and presented in detail. As discussed previously these are generated by non–linear effects and hence the ability of the model to reproduce them is a critical test of how it can handle the cascade of energy to small scales. However as we will show the short wavelength of these waves and their modification by wind effects suggests that measurements to validate this aspect of the model will prove very difficult to make with a high level of accuracy.

The effect of wind forcing produced by a uniform steady wind upon the M_2 tide and its harmonics was examined in later calculations. A wind stress of 0.2Pa as used in XD97 was applied in these calculations. The generation of strong inertial oscillations which would persist in the solution and mask the steady wind induced response, was avoided by increasing the wind stress with a sine wave form corresponding to the first quarter of a sine curve (namely 0 to $\pi/2$) for 12 hours during the spin up period.

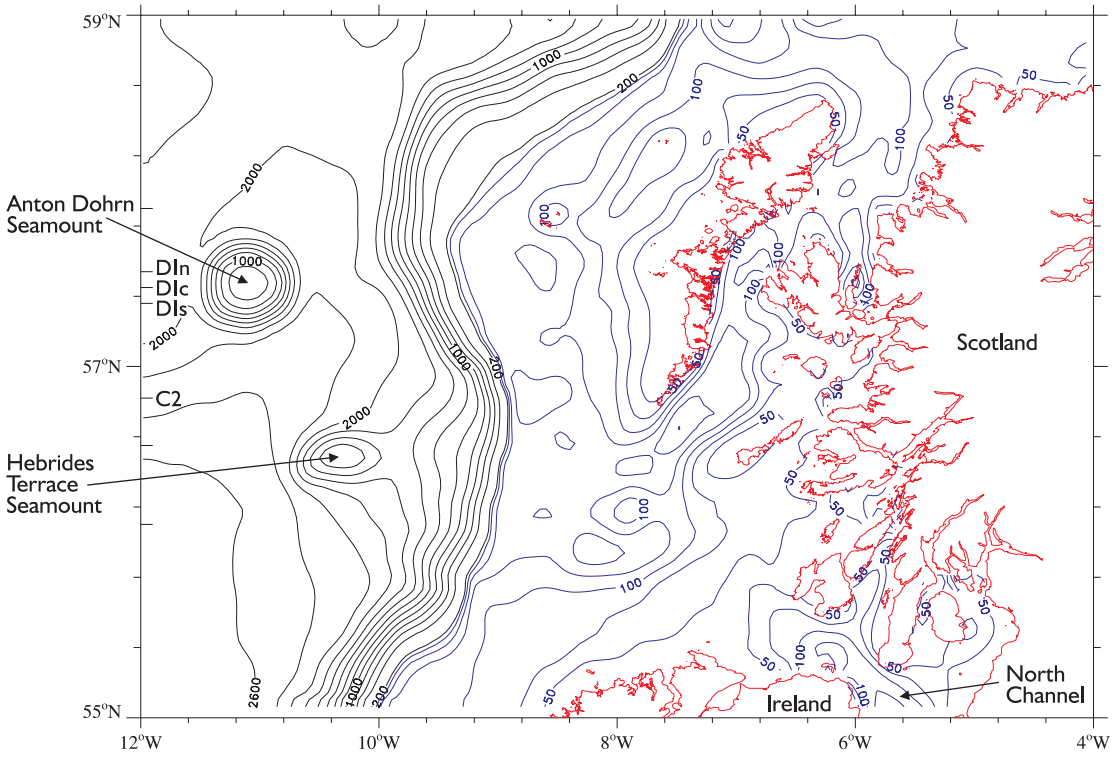

Fig. 1. Bottom topography (water depths in m) and area covered by the model. Cross sections where the influence of the wind upon the tide is examined in detail are denoted by lines C2, D1n, D1c and D1s. Geographical locations of regions named in the text are also shown.

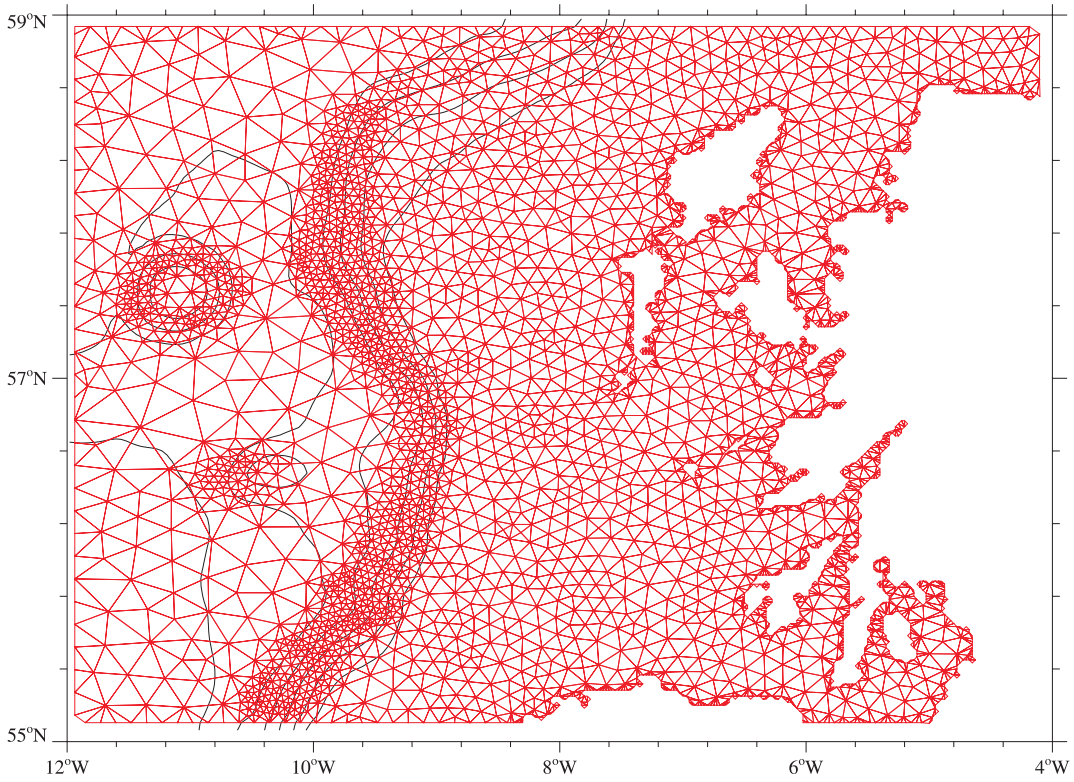

Fig. 2. The high resolution (see HD05a) finite element grid used in the model.

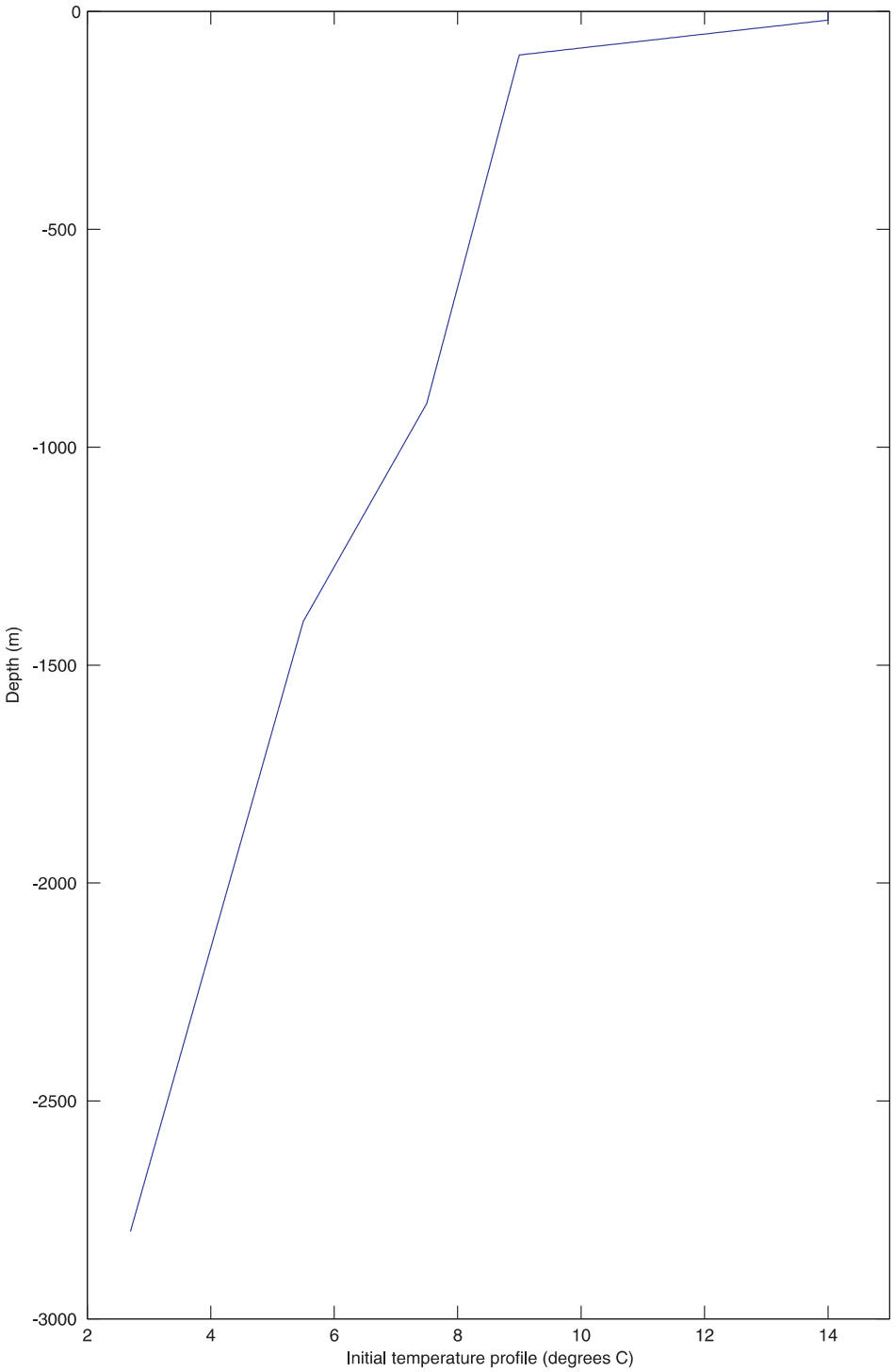

Fig. 3. Temperature profile (°C) used in the calculations.

Calc	Wind Duration Wind Direction
1	Tide Only
2	Short, N
3	Long, N
4	Short, S
5	Long, S

Table 1
Summary of various calculations. Note: Wind direction 'N' means a wind blowing towards the north.

3. TIDAL DISTRIBUTIONS

As considered in HD05a, barotropic tidal forcing produces a strong baroclinic tide that is separated from the total solution by subtracting a barotropic tide computed by running the model in a homogeneous form (see HD05a for detail). By this means changes in tidal current profile produced by viscous effects that are significant in boundary layers are removed from those due to internal pressure gradients, thereby leaving a true baroclinic signal. The alternative used in observational work of computing the baroclinic tide by subtracting the depth mean current, does not take account of viscous effects, and will not produce a true baroclinic profile in the boundary layer. This is discussed later in connection with the M_6 tide. By harmonically analysing the resulting baroclinic tide, the residual current and the M_2, M_4 and M_6 components of the baroclinic tide were determined. A similar approach was applied in the wind forced case. In a homogeneous tidal model, the residual current, namely the tidal residual and the higher harmonics M_4 and M_6 are due to non–linear effects. In the stratified case differential tidal mixing between shelf and shelf edge leads to a shelf edge front, with an across shelf density gradient. Associated with this density gradient is an along frontal flow in addition to any flow induced by wind forcing. However this aspect of the solution is beyond the scope of the present paper.

Previous tidal calculations (XD97 and HD05a) showed that the presence of topographic features such as the Anton Dohrn offshore seamount at about 57.5°N (Fig. 1) influences the local distribution of the M_2 internal tide. In addition Lamb (2004) showed that topographic features such as seamounts had an important role in generating higher harmonics. For these reasons we will initially examine the distribution of the M_2 tide and its higher harmonics in this area. To be consistent with HD05a, the same cross sections namely D1n, D1c and D1s (Fig. 1) are considered to determine the spatial distribution of the higher harmonics. However since the M_2 baroclinic tidal distribution at all cross sections was examined in HD05a, this component will only be considered in detail at cross section D1n.

Considering initially the M_2 baroclinic tidal current at cross section D1n. It is evident from Fig. 4 that on the shelf a surface and bottom intensification of M_2 baroclinic current amplitude which is indicative of a first mode internal wave is evident although higher modes with reduced amplitude also occur. A bottom intensification of the internal tide at the shelf break, extending down the slope is also apparent. These regions of internal tide generation are associated with areas of critical slope, where the shelf slope $\partial h/\partial x$ matches the internal wave slope S, given by $S^2 = (\omega^2 - f^2)/(N^2 - \omega^2)$ with ω the M_2 tidal frequency, f Coriolis and N buoyancy frequencies, and an enhanced internal tide is generated (see Vlasenko et al. 2005, for details). Obviously in the model the topography and hence $\partial h/\partial x$ varies down the slope. Also due to bottom boundary layer mixing N varies from its initial value in a complex manner depending upon local tidal turbulence intensity (see later) which depends upon both barotropic and baroclinic bottom currents. These changes in $\partial h/\partial x$ and S exhibit significant small scale variability and hence appreciable local changes in internal tide intensity occur. In addition there is internal tide propagation from the Anton Dohrn seamount onto the shelf slope (see below and XD96). Comparison at other cross sections (not presented) did however show that the extent of this downslope region of intensified bottom current varied from section to section in the region of the seamount. This is to be expected since $\partial h/\partial x$ shows significant variability in the seamount region, and bottom turbulence and hence N changes over relatively small distances (see later).

The variation in the magnitude of the M_2 internal tide over small horizontal distances (see separation of cross sections D1n, D1c, D1s in Fig. 2) in the Anton Dohrn region is because both super–critical and sub–critical internal tides are generated along the shelf slope and on the seamount sides, producing internal tides that propagate both onto the shelf and into the ocean (see XD96 for detail). As shown in XD96 the exact location and topography of the seamount was responsible for the offshelf distribution of the internal tide. Further to the south of the seamount (see cross section C2), where the slope is steeper, the region of maximum M_2 internal tide occurs down the slope in deeper water (not shown). In the shelf break region, a surface intensification occurs, with a slight increase on the shelf at depth, suggesting that there is little on shelf propagation of the internal tide at cross section C2.

Contours of the u current amplitude at the M_4 frequency in the Anton Dohrn region show (Figs. 5a–c), an intensification at depth along the eastern side of the seamount at cross section D1n (Fig. 5a). This location corresponds to the area of strong M_2 baroclinic tidal currents (Fig. 4), which show significant spatial variability. Consequently the non–linear momentum advection terms which transfer energy to higher harmonics are a maximum in this region and give rise to this strong M_4 signal. Similarly a local increase in M_4 tidal current is apparent at the sea surface and sea bed to the east of the seamount and near the shelf break where there is an appreciable lateral gradient in the M_2 tidal current (Fig. 4). Besides the non–linear momentum advection terms, other terms such as time varying eddy viscosity (Davies and Lawrence 1994) can give rise to higher harmonics of the tide, although these were appreciably less. In addition quadratic friction can generate higher harmon-

ics, although this is the M_6 rather than M_4 component (see later).

At cross section D1c the region of maximum M_4 current amplitude is located on the western side of the seamount (Fig. 5b) in the region of significant gradients in the M_2 baroclinic tidal current (not shown but see HD05a). A weaker signal is evident (Fig. 5b) on the eastern side due to the reduced intensity of the M_2 tide in this region compared to previously (Fig. 4). A mid–water M_4 maximum current is apparent at the top of the shelf slope (Fig. 5b) corresponding to a region of rapid M_2 tidal current variation.

At the southern edge of the seamount (cross section D1s) there is a local enhancement of the M_4 tidal current on either side of the seamount and in the shelf break region (Fig. 5c). These areas correspond to regions of enhanced M_2 u–current amplitude (not shown but see HD05a). At cross section C2, there is a small (of order 3 cm s^{-1}) M_4 tidal current amplitude at the shelf break and along the shelf slope (not shown) in regions where the M_2 tidal current is significant.

The distribution of the M_6 tidal current amplitude along cross section D1n (Fig. 6) is comparable to that for the M_4 tide (Fig. 5a), although its amplitude is about half that of the M_4 tide (compare Figs. 5a and 6). Similarly at the other cross sections (not shown) the spatial distribution of the M_6 tide is comparable to that for M_4, although its amplitude is about half. This suggests that it is non–linear interaction in regions where the M_2 internal tide is largest and has a strong spatial variability (significant gradient) that is responsible for the generation of higher harmonics. Away from the near bed region the non–linear momentum advection terms which transfer energy from the M_2 to M_4, also move energy to the M_6 tide. However, in the near bed region the quadratic friction term is the dominant mechanism and moves energy from the M_2 to M_6 frequency. By generating an M_6 baroclinic tide by removing the barotropic component using a homogeneous calculation from the total tide it is possible to isolate the M_6 baroclinic tide. The alternative that would have to be used in the case of observational data would be to subtract a depth mean M_6 tidal current from the total, which would clearly only partially remove the barotropic M_6 tide. Consequently a rigorous validation of the M_6 component against observations would be very difficult. In addition since M_6 is generated in the nearbed region through bed friction and turbulence, detailed measurements of bed roughness and thickness of the turbulent bottom boundary layer would be required (see later).

As the internal tide upwells and downwells over the steep topography tidal mixing occurs and this influences the temperature field. Although the extent of the displacement of the temperature surfaces varies with depth below the surface, it is useful to examine its spatial variability at a given depth. To this end the model was run for a significantly longer period of time (namely 20 tidal cycles) to allow tidal mixing and tidally produced turbulent kinetic energy (t.k.e.) to become established. In essence tidal mixing in the bottom boundary layer changes the temperature field from its initial prescribed value to one which is consistent with the internal tidal distribution and the turbulent Ekman lower layer.

Away from the Anton Dohrn Seamount and the shelf edge region a near uniform spatial distribution of temperature was found at 600 m (Fig. 7a). Since this depth is above the top of the seamount, the reduction in temperature is associated with enhanced vertical mixing above the seamount (see later). Enhanced up–welling and vertical mixing at the shelf edge region to the north of 57°N leads to regions of cold water, the across shelf extent of which varies with position (Fig. 7(a)). It is evident from Fig. 7a that it is largest in the region to the north–east of the seamount where XD96 showed there is a significant M_2 tidal energy flux both along and across the depth contours. In the region of cross section C2 there appears to be a region of slightly warmer shelf edge water at 600 m depth. As the shelf slope is different at this location compared to cross sections D1 this gives rise to a maximum internal tidal current at about 1200 m depth rather than higher up the slope (of order 600 m) found farther north. Differences in location at depth of maximum internal tidal current generation will produce differences in boundary layer mixing that will influence the temperature distribution. Although a detailed study of this is beyond the scope of this paper we will briefly consider the spatial variability of t.k.e.

At a depth of 1200 m there is more horizontal spatial variability in the temperature field (not shown), associated with small scale variations in mixing due to spatial changes in tidally produced turbulence. Contours of log10 t.k.e. along the shelf slope show (Fig. 7(b)) significant spatial variability. To be consistent with the temperature distribution plot, these contours correspond to a depth of 1200 m below the surface, rather than a height above the sea bed that is more appropriate in the case of bed generated turbulence. Since it is not possible, due to the highly non–linear nature of the processes producing t.k.e. to partition it into a barotropic and baroclinic part, these contours represent total turbulent kinetic energy. A major source of this on the upper part of the shelf slope region is due to the barotropic tide.

However, as shown by Xing and Davies (1996a,b) at depth, along shelf slopes it is a maximum in nearbed regions where the internal tide is generated. The strong maximum at 1200 m, in the shelf edge region (Fig. 7b) at the location of strong internal tides at cross section C2 shows that this is associated with the internal tide production in this area, at this depth. As discussed above internal tide production was evident in the across slope distribution of u–current amplitude at this depth. The significant spatial distribution of t.k.e. along the shelf slope region, shown in Fig. 7(b), illustrates that there will be appreciable variation in turbulence intensity measurements from one transect to another. In addition a high resolution model mesh resolution both across and along the shelf slope is required. Appreciable small scale variations in t.k.e. are evident around

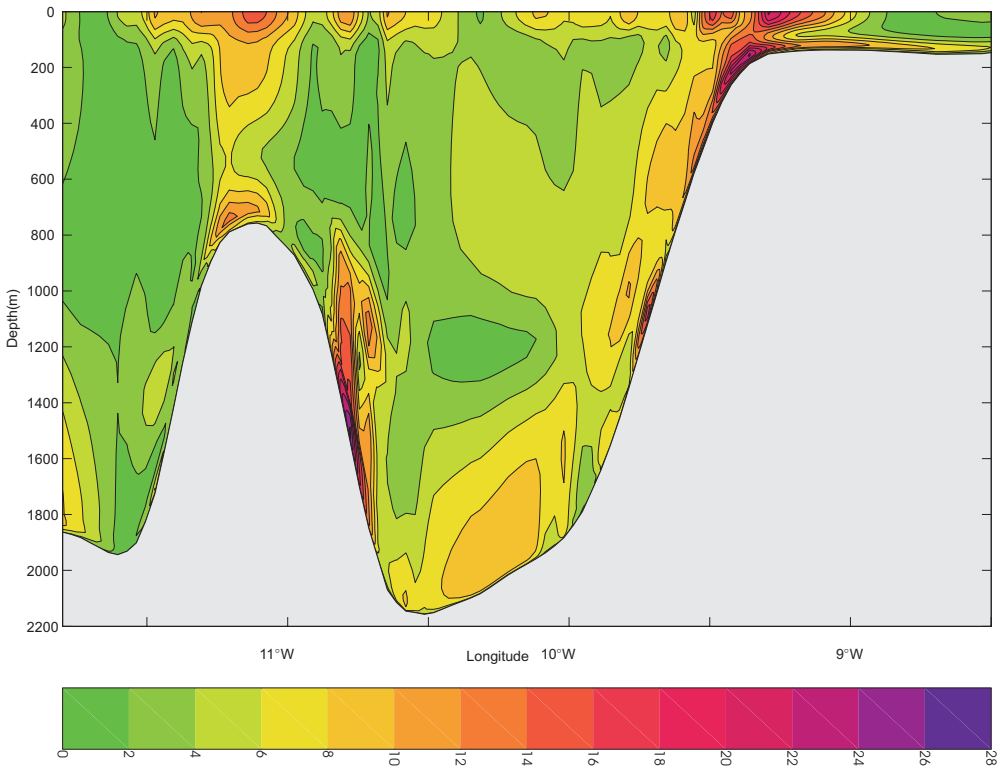

Fig. 4. Amplitude (cm s^{-1}) of the M_2 harmonic of the u–component of the baroclinic tide along cross section D1n.

the Anton Dohrn Seamount, with the region of enhanced turbulence to the north (Fig. 7b), associated with the shallower water in this area. A similar feature is just evident on top of the Hebrides Terrace Seamount (Fig. 7b).

To examine the depth and lateral variation of t.k.e. in more detail, cross section plots of log10 t.k.e. were computed along cross sections D1n, D1c, D1s (Figs. 8a to 8c) and C2, at the time corresponding to the internal tide contours shown previously. Contours of t.k.e. at cross section D1n, exhibit (Fig. 8a) enhanced turbulence in the near bed region, particularly at the shelf break and at depth along the eastern edge of the seamount where internal tide generation is a maximum (Fig. 4a). At cross section D1c the region of maximum t.k.e. is situated at depth on the west side of the seamount (Fig. 8b) in the region of strong M_2 internal tide production. A region of intensified turbulence is evident at the shelf break with patches of intensified turbulence down the shelf slope in areas corresponding to internal tide generation. Similar patches of intensified turbulence occur on both the western and eastern side of the seamount and along the shelf slope at cross section D1s (Fig. 8c) in regions of enhanced internal tide. At cross section C2, where the internal tide at the shelf break is small near bed t.k.e. (not shown) is small and of limited lateral extent.

The effect of increased turbulence energy in these regions is to enhance nearbed mixing thereby reducing the buoyancy suppression of turbulence in the nearbed region. A consequence of this is that in some areas near bed turbulence increases with time. This time increase was found to be particularly large and extend away from the near bed at cross sections D1s and C2. A comparison of the time variation of t.k.e. at cross section D1s (not presented) shows that the intensity and lateral extent of turbulent energy along the seamount slope and in the shelf edge region where the internal tide is a maximum rapidly grows with time. Similarly at cross section C2 (not shown) there is a rapid increase at a depth of 1200 m, associated with the strong internal tide in this region. As discussed previously in connection with Fig. 7b, at this depth the maximum turbulence energy in the shelf edge region occurs at cross section C2. The fact that these regions of maximum t.k.e. occur at locations of maximum internal tidal current amplitude shows that in the shelf slope region there will be other maxima at different positions and depths. Consequently in the shelf slope region there will be considerable small scale variation in the location of strong t.k.e. regions. This clearly shows that any measurement strategy aimed at determining turbulence energy data sets for model validation will require high resolution sampling.

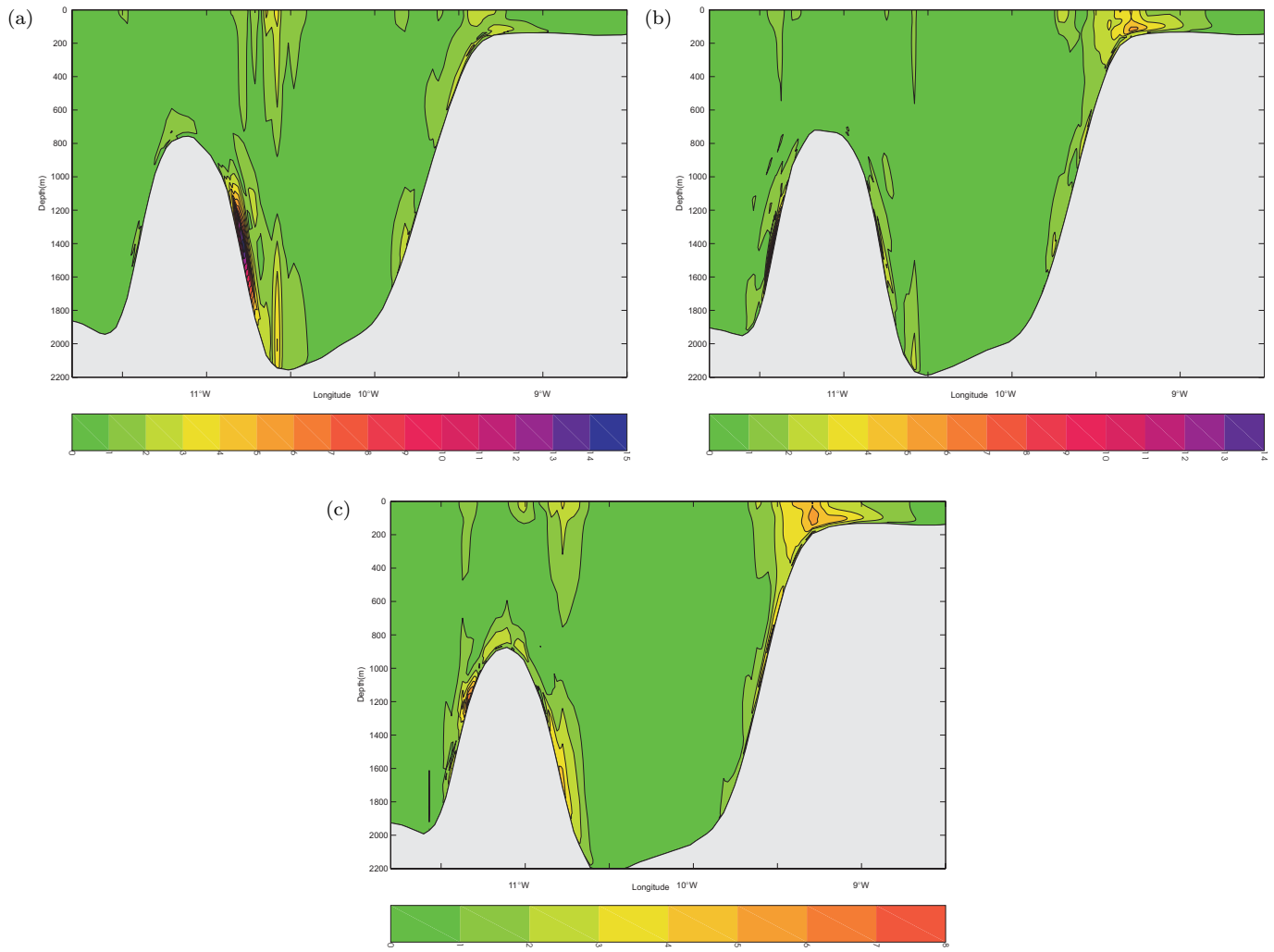

Fig. 5. Amplitude (cm s^{-1}) of the M_4 harmonic of the u component of the baroclinic tide at cross sections (a) D1n, (b) D1c, (c) D1s.

4. WIND FORCING EFFECTS

4.1. *Wind towards the north (a down–welling favourable wind)*

In order to determine the influence of wind effects upon the internal tide, calculations were performed with winds of short and long duration towards the north (Calcs 2 and 3) and the south (Calcs 4 and 5). A summary of the calculations is given in Table 1. After the initial ramping up period a fixed time and space invariant wind stress of 0.2Pa was used in all calculations, with open boundary barotropic tidal forcing as in Calc. 1.

The effect of short term wind forcing was enhanced mixing in the surface layer with an associated weakening of the thermocline in the near surface (of order 100 m) layer. However below this layer there was little change in the tidally averaged (over an M_2 tidal cycle) temperature field.

To determine the effect of wind upon tidal u–current amplitude along cross section D1n, differences in amplitude with and without wind forcing were computed for each constituent (Figs. 9a–c). Contours of this difference for the M_2 internal tide away from the shelf show (Fig. 9a) that the change in the M_2 internal tide is mainly restricted to the surface layer where the temperature and hence density field has been changed by the wind. The largest effect occurs in the surface layer above the seamount where the current due to the internal tide was a maximum (Fig. 4). On the shelf besides changes in the M_2 internal tide at the surface there are some changes at depth. This is due to enhanced mixing arising from an increase in bottom turbulence due to wind induced bottom currents in shallow water. On average these changes were of the order of 5 cm s^{-1}, (Fig. 9a) compared with the M_2 internal tidal current amplitude (Fig. 4) of order above 20 cm s^{-1}. Namely a change of over 20%. Changes in the u–current amplitude of the M_2 internal tide at other cross sections was not appreciably different to that shown in Fig. 9a.

For the M_4 component, the most significant modifications (Fig. 9b) occur in the surface layer particularly in the shelf break region where the M_2 tidal current (Fig. 4) is

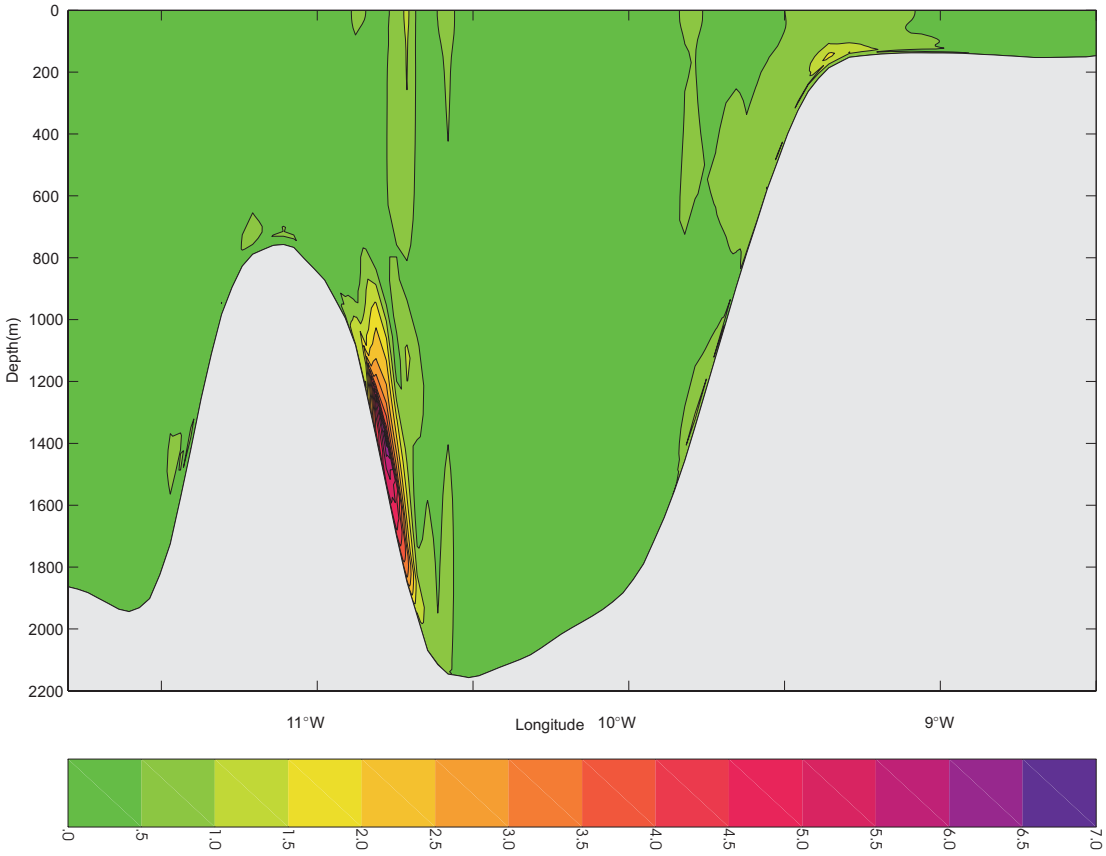

Fig. 6. As Fig. 4 but for the M_6 harmonic at cross section D1n.

largest. As discussed previously the M_4 is produced by the non–linear interaction of the M_2 tide with itself. Consequently changes in M_4 will be largest in regions where the largest changes occur in M_2, namely the surface layer. Typically the changes in M_4 are only of the order of 1 cm s^{-1} (Fig. 9b), although this is significant in the surface layer where the M_4 tidal current is only about 3 cm s^{-1} (Fig. 5a). At depth, along the eastern side of the seamount, the M_4 changes by about 1.4 cm s^{-1}. In this area, the M_4 current is appreciable (up to 14 cm s^{-1}) (Fig. 5a), and this change reflects the small shift in M_2 tidal current maximum at depth (Fig. 4) in this region due to the small difference in temperature field produced by the wind. At other cross sections (not shown) comparable changes to the M_4 tidal current amplitude occur in the surface layer, with small changes at depth in regions where the M_4 tidal current is a maximum.

The wind induced difference in the M_6 tidal current along cross section D1n (Fig. 9c) shows a comparable distribution in the surface layer to that computed for M_4, although with a significant (of order 50%) reduction in magnitude. Similarly at depth the region of change corresponds to that found for the M_4 tidal current (compare Figs. 9b and c). A study of the M_6 tide shows that in this region the M_6 arises from M_4 and M_2 interaction, with these changes reflecting differences in the M_2 distribution. As for M_4, at other cross sections (not shown), the M_6 changes in the surface layer are comparable to those shown in Fig. 9c, with modifications at depth occurring in regions where the M_6 current is a maximum.

A consequence of applying a short duration wind forcing is that the major change in the density field only occurred in the surface layer. However, when a wind stress of 0.2 Pa was applied for 30 tidal cycles, XD97 found that there was appreciable mixing along the shelf slope region which affected the generation and offshelf propagation of the internal tide. As shown in XD97 this influenced the M_2 tide at depth. To examine this in more detail, the previous calculation was repeated with the wind applied for 20 tidal cycles (Calc. 3).

The result of applying the wind stress for a longer period is appreciably more mixing in shallow water than found in the tide only calculation together with a weakening of the surface thermocline (Fig. 10a) compared to the short wind period calculation. It is evident from Fig. 10a, that at depth, particularly in the regions adjacent to the sea bed, enhanced mixing has changed the local density gradient. This is in part due to the wind field, but tidal mixing also contributed to the mixing at depth in slope regions, due to the extended time integration.

Contours of the time averaged (over a tidal cycle) differences in the temperature distribution at 200 m between that with tide and wind and tide alone are given in Fig. 10b.

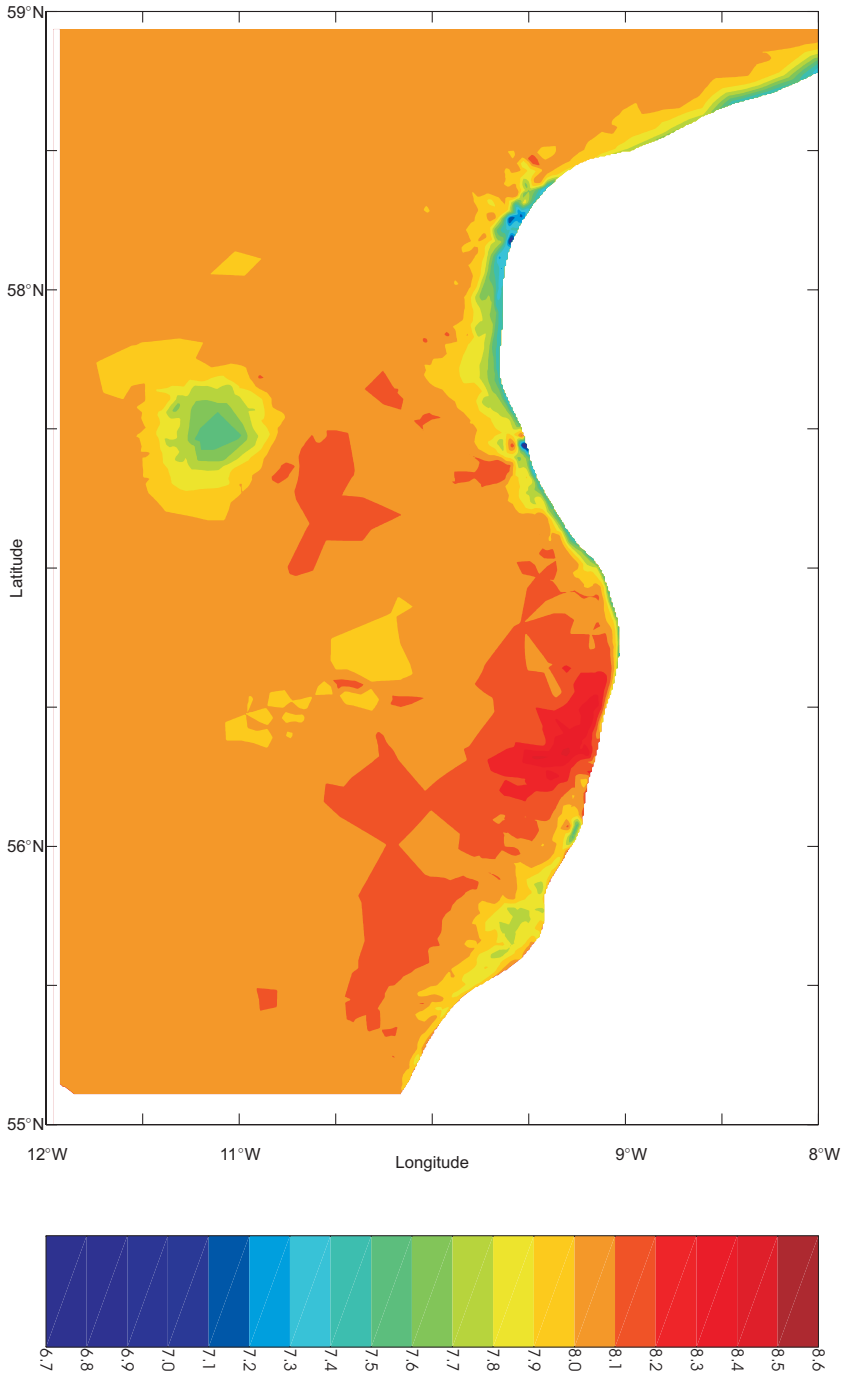

(a)

Fig. 7. (a) Horizontal temperature distribution (°C) at a depth of 600 m below the surface, (b) horizontal distribution of $\log_{10}$ t.k.e. ($m^2\ s^{-2}$) at a depth of 1200 m below the surface. Both were derived from a long tidal integration.

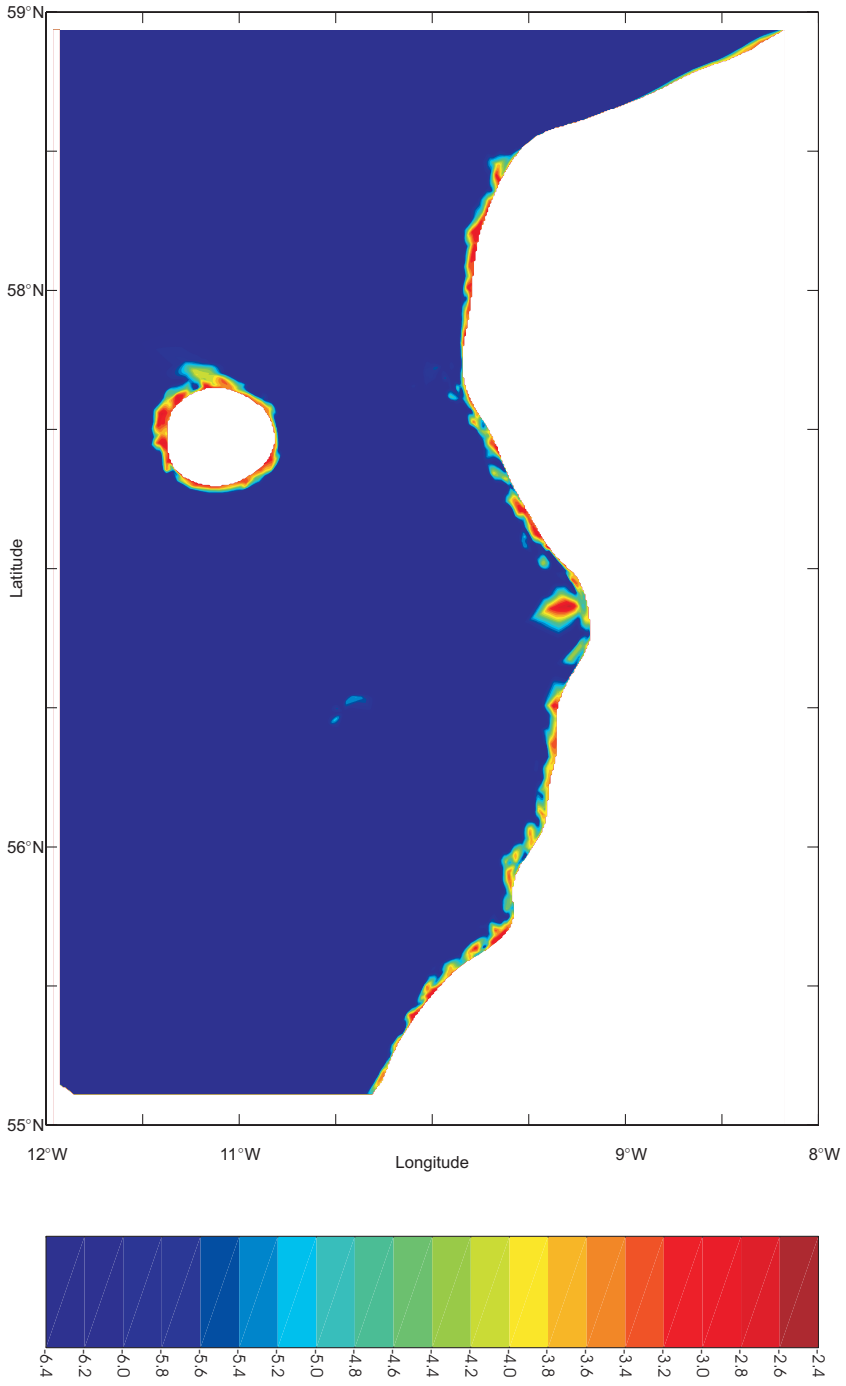
59°N
58°N
56°N
55°N
Latitude
12°W
11°W
9°W
8°W
Longitude
-6.4
-6.2
-6.0
-5.8
-5.6
-5.4
-5.2
-5.0
-4.8
-4.6
-4.4
-4.2
-4.0
-3.8
-3.6
-3.4
-3.2
-3.0
-2.8
-2.6
-2.4

(b)

Fig. 7. (Contd.)

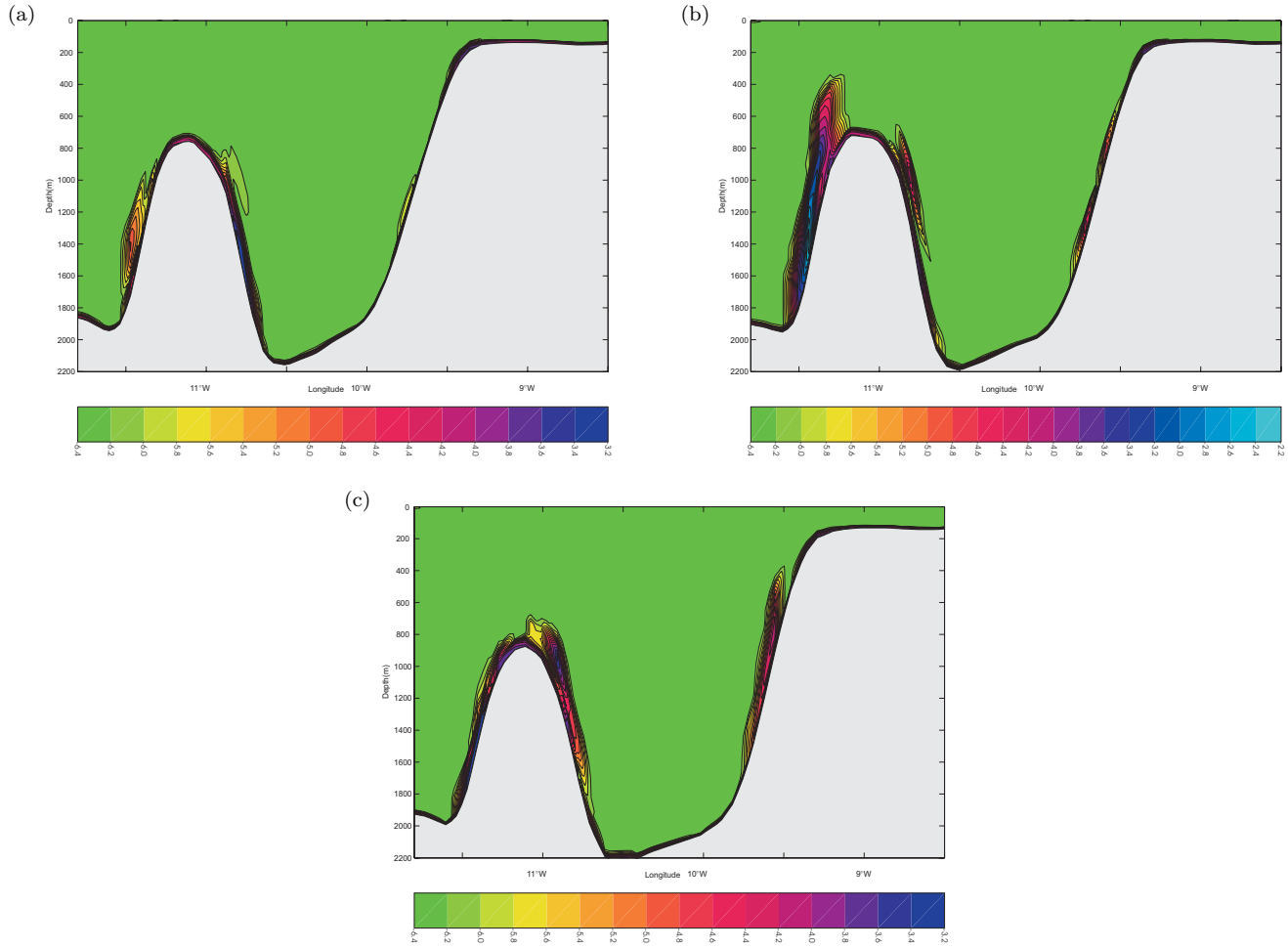

Fig. 8. Cross sections of $\log_{10}$ t.k.e. (m^2 s^{-2}) at cross sections (a) D1n, (b) D1c, (c) D1s from a short tidal integration.

In the case of a downwelling favourable wind, in a coastal region, and as found by XD97 at the shelf edge warm surface water downwells to depth and gives rise to an increase in temperature. Some shelf edge regions of increased temperature at depth are clearly evident in Fig. 10b, although elsewhere the temperature is reduced. In the deep ocean, as expected there is little change in temperature. The existence of patches of increased/decreased temperature in the shelf edge region shows that the three dimensional temperature response to wind forcing is more complex than that found by XD97 in a cross–sectional model. In three dimensions the internal tide can propagate both across and along the shelf edge. In addition the vertical velocity associated with the wind induced flow is more complex than in a cross–sectional model. This leads to greater spatial variability in the internal tidal signal and the associated mixing of tidal and wind origin. In addition alongshelf flows of wind origin can advect water from one region of tidal mixing to another. A process that is not included in a cross–sectional model.

As in the short wind period calculation, contours of the difference in u–current amplitude along cross section D1n for the M_2, M_4 and M_6 components were determined. For the M_2 tide it is evident (Fig. 11a) that there is no substantial change on the shelf. However an appreciable change in M_2 baroclinic tidal current amplitude (Fig. 11a) has occurred in the surface layer above the shelf break and at the top of the shelf slope associated with the change in stratification. In addition, near the foot of the slope an appreciable M_2 internal tide is produced (Fig. 11a) associated with the change in stratification. Also a strong internal tide was produced along the western side of the seamount (Fig. 11a) a region where previously (Fig. 4) there was no internal tidal signal. The reason for the appearance of the internal tide in these areas is due to a local change in stratification arising from prolonged tidal and wind induced mixing. Comparable changes in the stratification at depth, at other cross sections D1c and D1s (not shown) gave similar changes.

The modification of the M_2 internal tide gives rise to a similar pattern of change in the M_4 component (Fig. 11b). However the magnitude of the change (Fig. 11b) is small (of order up to a maximum of 2.5 cm s^{-1}). As in the short duration wind case (Calc. 2, Table 1) there is an appreciable change in the M_4 near surface tidal current amplitude due to wind mixing in the surface layer affecting the M_2 tide. In addition there is a small M_4 tidal signal at depth along the shelf slope and on the western side of the seamount in

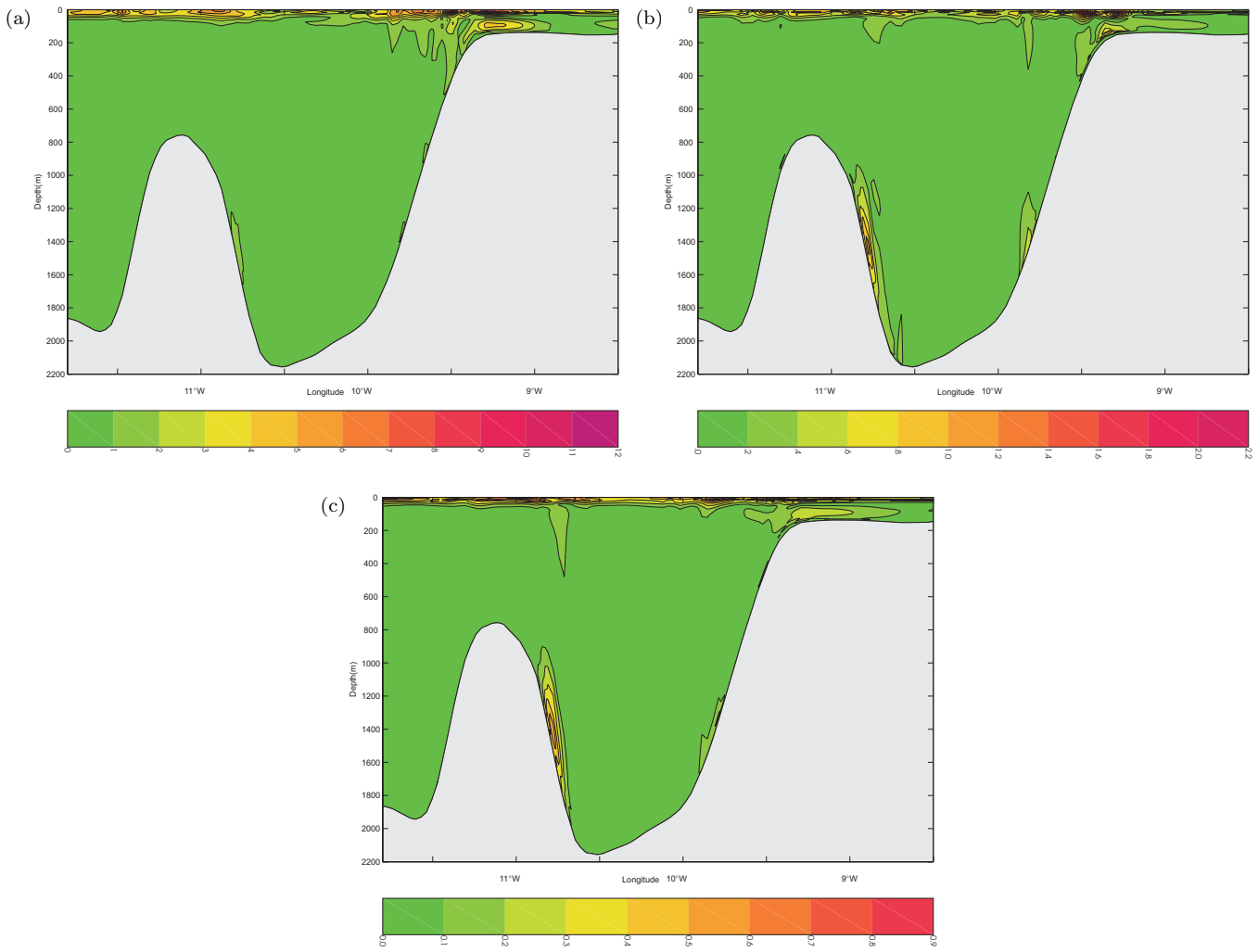

Fig. 9. Contours of the difference in baroclinic tidal amplitude (cm s^{-1}) between the wind (0.2 Pa towards the North) and tidal solution and a tide only solution for short wind duration forcing (Calc. 2) at cross section D1n, for (a) M_2, (b) M_4 and (c) M_6 frequency.

the regions where there is an M_2 internal tidal signal in the longer duration wind case. Similar large scale changes in the M_4 current amplitude occurred at other cross sections (not shown). Although the large scale distribution was similar, the exact location and magnitude varied between cross sections due to differences in topography and mixing.

As in the short duration calculation, the largest wind induced modification of the M_6 tidal current arises in the surface layer (Fig. 11c). At depth the largest change occurs in the slope region where the modification of the M_2 and M_4 tide has been greatest. As considered previously this shows that M_6 is produced by the non–linear interaction of M_2 and M_4 in these areas, although changes in bottom friction due to changes in M_2 will have an effect.

As shown in the short wind forced calculation, the introduction of a wind stress influences mixing and hence turbulence energy. How this is modified by the longer duration wind was examined in terms of contours of t.k.e. from cross section D1n (Fig. 11d). To determine to what extent the presence of a long (20 tidal cycle) wind stress of 0.2 Pa towards the north has upon the turbulence energy distribution, contours of t.k.e. were plotted at the various cross sections (Fig. 11d). The presence of the surface wind stress gives rise to an enhanced layer of surface and on–shelf turbulence at cross section D1n (Fig. 11d) that was not present in the tidal solution. In addition the distribution of t.k.e. in the seamount and shelf slope region changes, due to wind induced mixing, and corresponding changes in the density field. This modification of the density field affects the location and intensity of the internal tide (Fig. 11a) giving rise to the differences that are evident between Figs. 11d and 8a. A detailed study (not presented) based on other cross sections shows similar changes in mixing and t.k.e. distribution from one cross section to another. However, the spatial variability of the mixing from one cross section to another appears to be enhanced by the presence of the wind. This series of calculations shows that the distribution of the internal tide and its higher harmonics is modified by a modest wind stress of 0.2 Pa. With short duration forcing this is confined primarily to the surface layer. How-

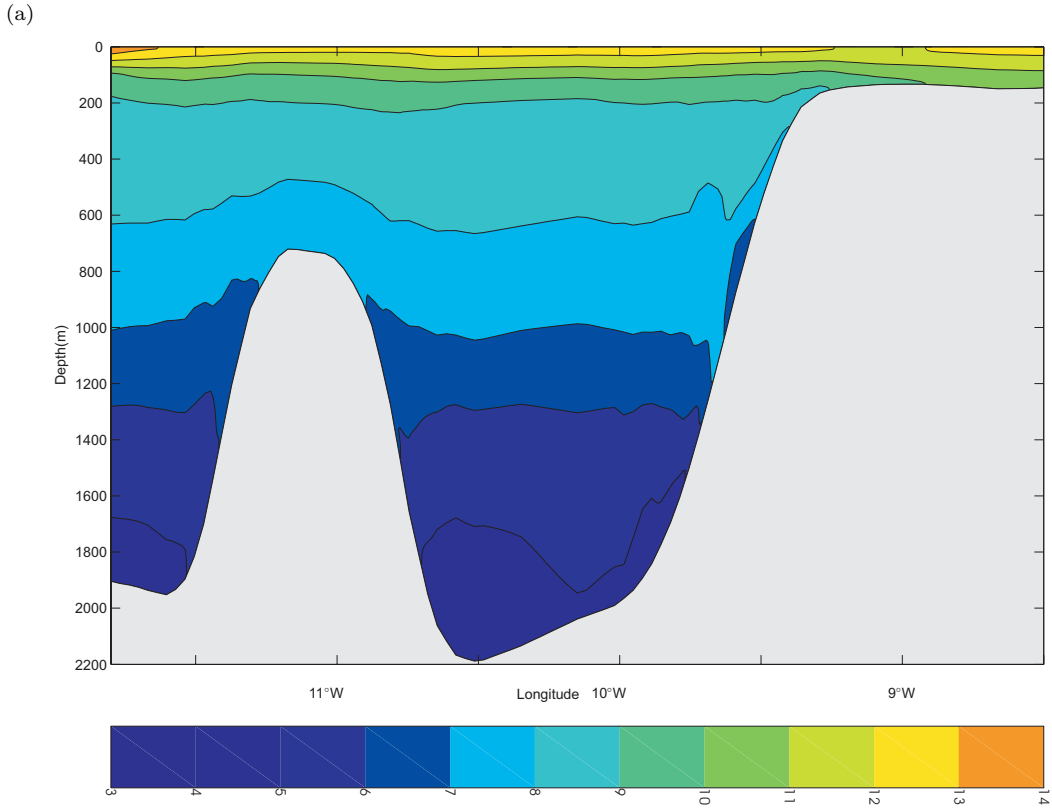

Fig. 10. (a) Temperature contours (°C) at cross section D1n from a tide and wind (0.2 Pa towards the North) integration, (b) changes in temperature (°C) at 200 m for a tide and north wind (0.2 Pa) minus a tide only calculation, (c) as (b) but for a south wind.

ever, on the 10 day time scale it modifies the stratification along shelf slopes, and in particular those associated with off–shelf seamounts.

4.2. *Wind towards the South (an up–welling favourable wind)*

In this section results are presented from calculations performed with both a short duration (Calc. 4) and longer duration (Calc. 5) up–welling favourable wind stresses of 0.2 Pa. As previously temperature contours along various cross sections (not presented) show enhanced surface mixing, comparable to those found in Calc. 2. Some slight differences in the region of topographic slopes were evident due to differences in mixing with an up–welling wind compared to down–welling. The change in M_2 tidal current amplitude (Fig. 12) was not significantly different from that found with the down–welling wind (compare Figs. 9a and 12) except for an increase in intensity and lateral extent in u surface current amplitude at about 10°W. This is due to changes in shelf slope stratification which influences the generation region and subsequent propagation of the M_2 internal tide. Comparable changes to those shown in Fig. 12 occurred at other cross sections. For the M_4 and M_6 components (not shown), the dominant features of the distribution and magnitudes of the changes were not appreciably different to those shown in Figs. 9b,c.

As to be expected there is appreciably more mixing in the slope regions, in the 10 day wind forced calculation (Calc. 5). Calculations showed that wind forcing gives enhanced mixing in the slope region that subsequently spreads further into the ocean. Consequently this change in density influences both internal tide generation and propagation. As in the north wind case, contours of temperature change produced by the presence of the wind (Fig. 10c), show significant spatial variability in the shelf edge region. As this wind direction is up–welling favourable then a cross sectional model such as that of XD97 would give cooler water in the shelf edge region. Such regions are clearly evident in Fig. 10c with the majority of regions where warming occurred previously (Fig. 10b) replaced with cooler regions (Fig. 10c) due to the change in wind direction. As before there is no significant change in the deep ocean. However at about 57.5°N in both wind cases, there is an increase in water temperature, which arises from enhanced vertical mixing of tidal and wind origin at this location. The differences in mixing and density advection due to change in wind direction explains why there are differences in the M_2 internal tide under an up–welling compared to down–welling favourable wind (compare Figs. 11a and 13a). For the M_4 component the modification due to the up–welling wind shows (Fig. 13b) a larger change at depth and at a different position along the shelf slope than previously (Fig.

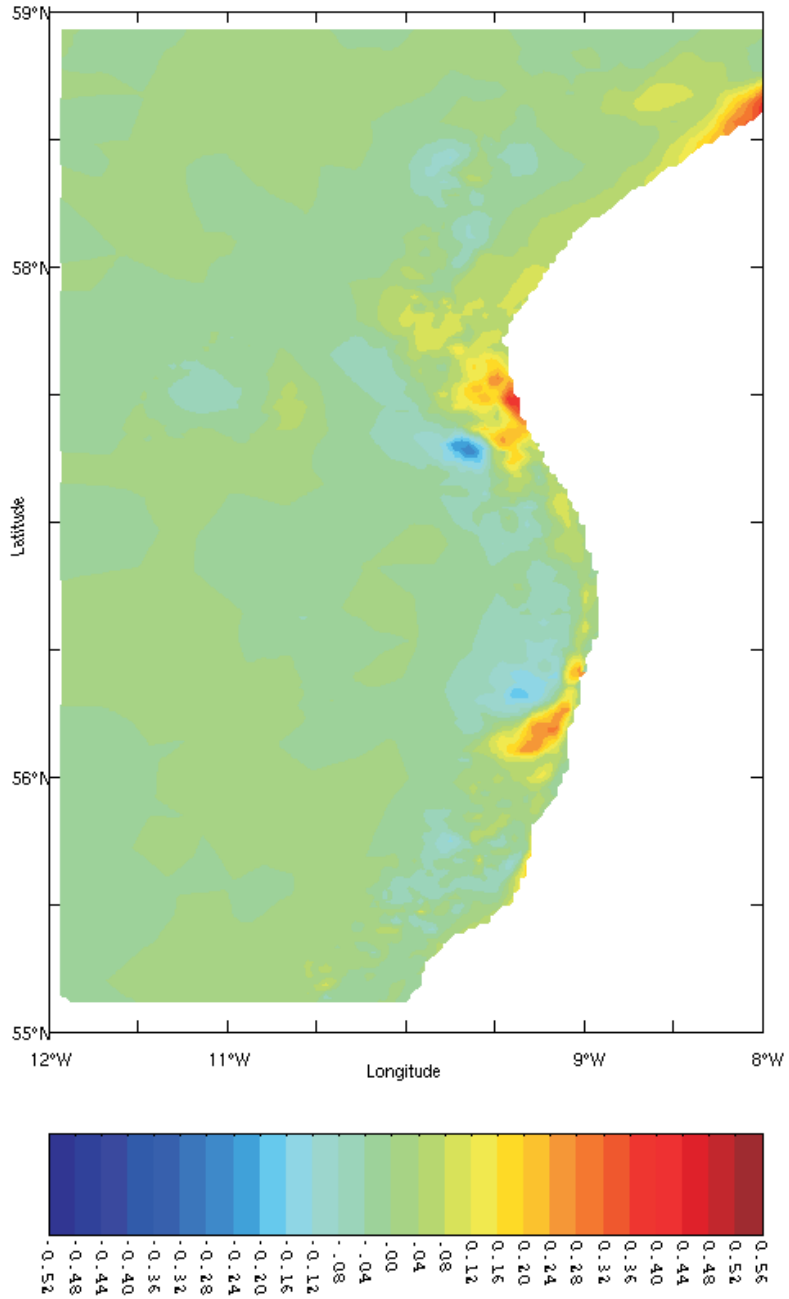

(b)

Fig. 10. (Contd.)

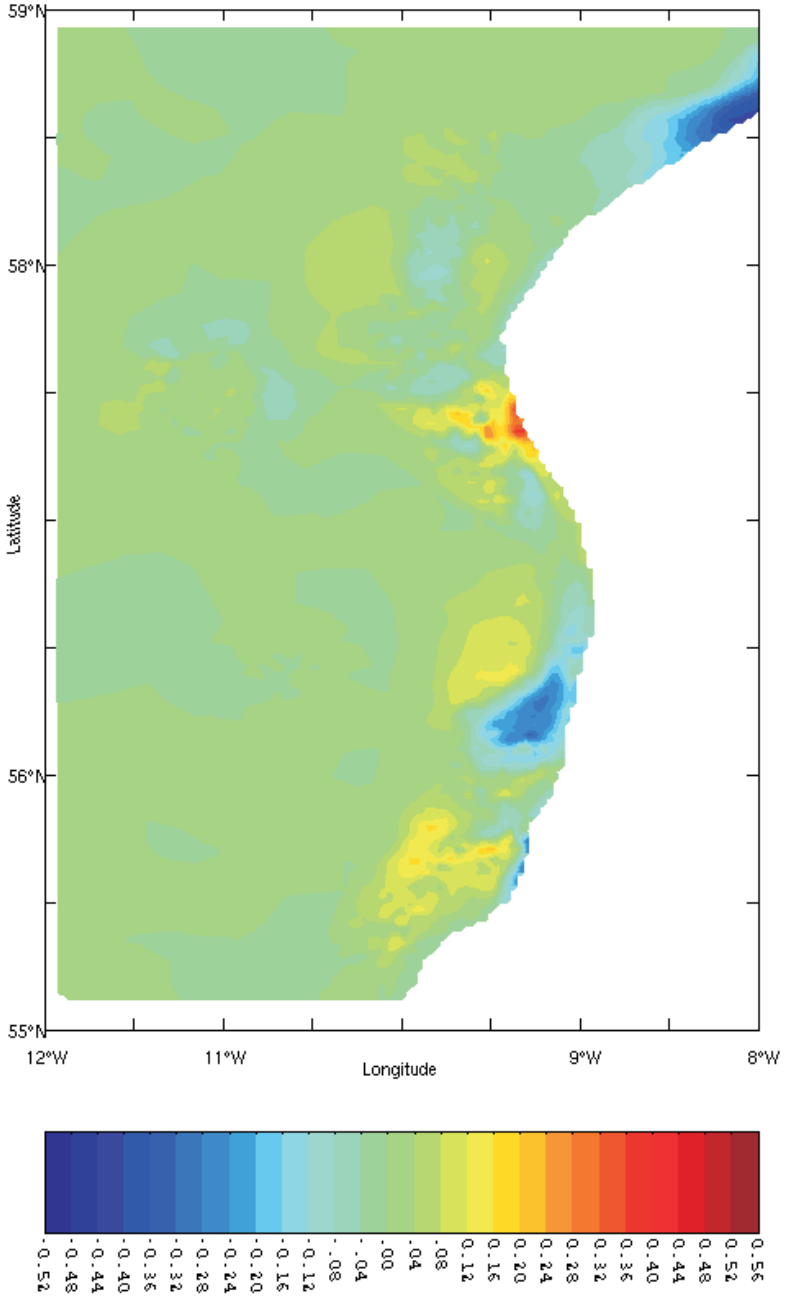

(c)

Fig. 10. (Contd.)

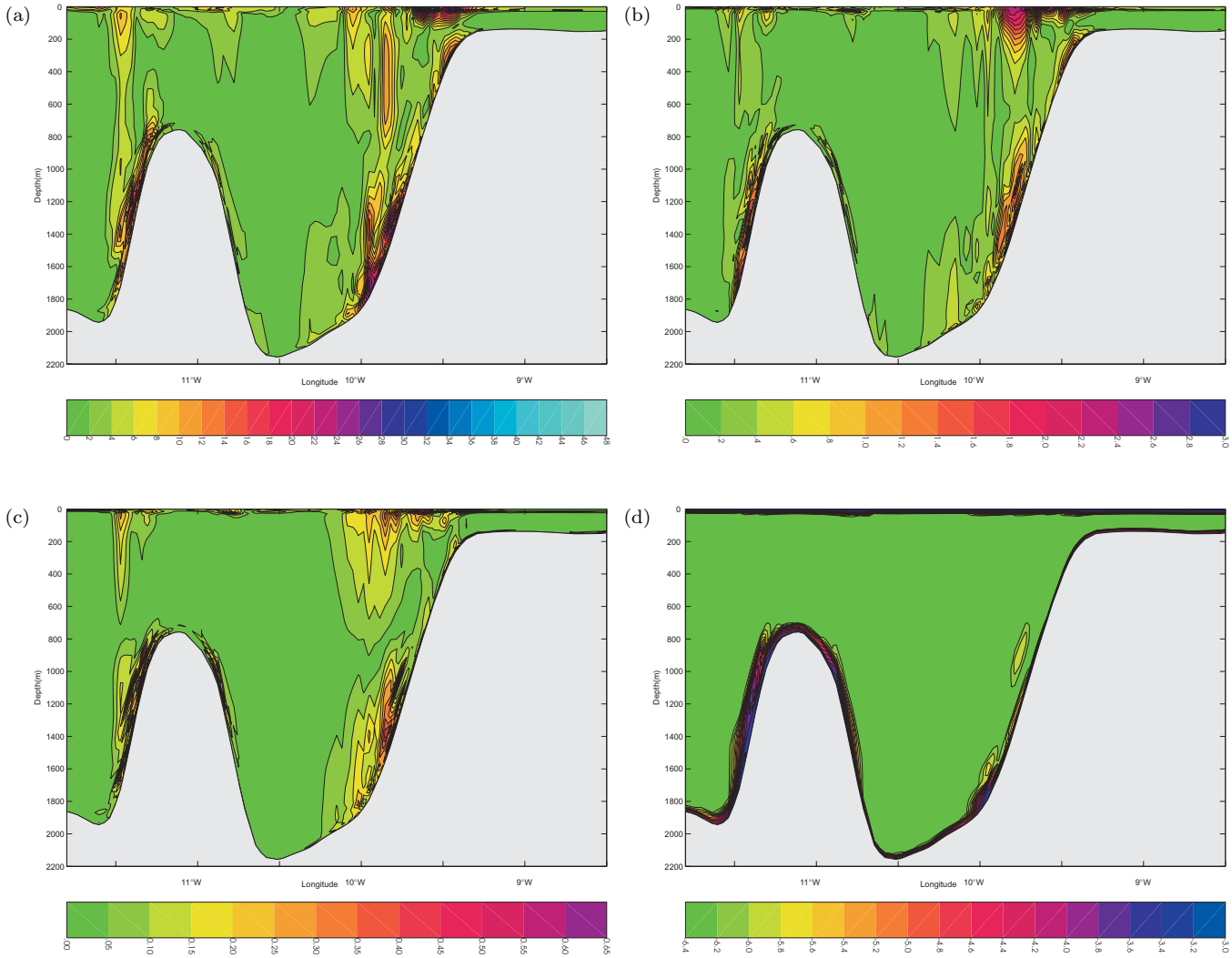

Fig. 11. As Fig. 9 but for a long integration (Calc. 3) with tide and wind (0.2 Pa towards the North), for (a) M_2, (b) M_4 and (c) M_6 tide with (d) $\log_{10}$ t.k.e. (m^2 s^{-2}).

11b). In addition the surface distribution and that on the western side of the seamount has been modified (Fig. 13b). As discussed previously these changes arise due to the different distribution of the M_2 tide computed with an up–welling rather than down–welling favourable wind. Similar modifications to the M_4 tide were found at other cross sections.

The dominant features of the distribution of the change in M_6 u–current amplitude (Fig. 13c) are comparable to those found with a down–welling wind (Fig. 11c), and on average are small, of the order of 0.5 cm s^{-1}. Although the large scale features are the same, on the smaller scale there are some differences due to differences in the distributions of the M_2 and M_4 tide. As discussed earlier the M_6 tide arises primarily from interaction between these components. At other cross sections the differences in tidal distribution are comparable to those shown at cross section D1n.

The calculations presented here show that on the longer time scale, wind effects substantially modify the M_2 component of the internal tide and its higher harmonics. Also the effect upon the internal tide is different under up–welling compared to down–welling wind forcing. Changes in the internal tide distribution arise not only in the surface layer but at depth where the wind field has modified the density field in the region of internal tide generation. In addition to changes in the M_2 component, the higher harmonics are modified to a different extent depending on wind direction.

5. CONCLUSIONS

The three dimensional calculations presented here, extend earlier work (XD97) which used a simple cross sectional finite difference model to study the influence of the wind. Such a slice model could not account for the along–shelf variation of topography, or for the presence of seamounts. In addition by using a proven finite element model (HD05a) with its ability to refine the grid in regions of rapid topographic change it is possible to resolve the

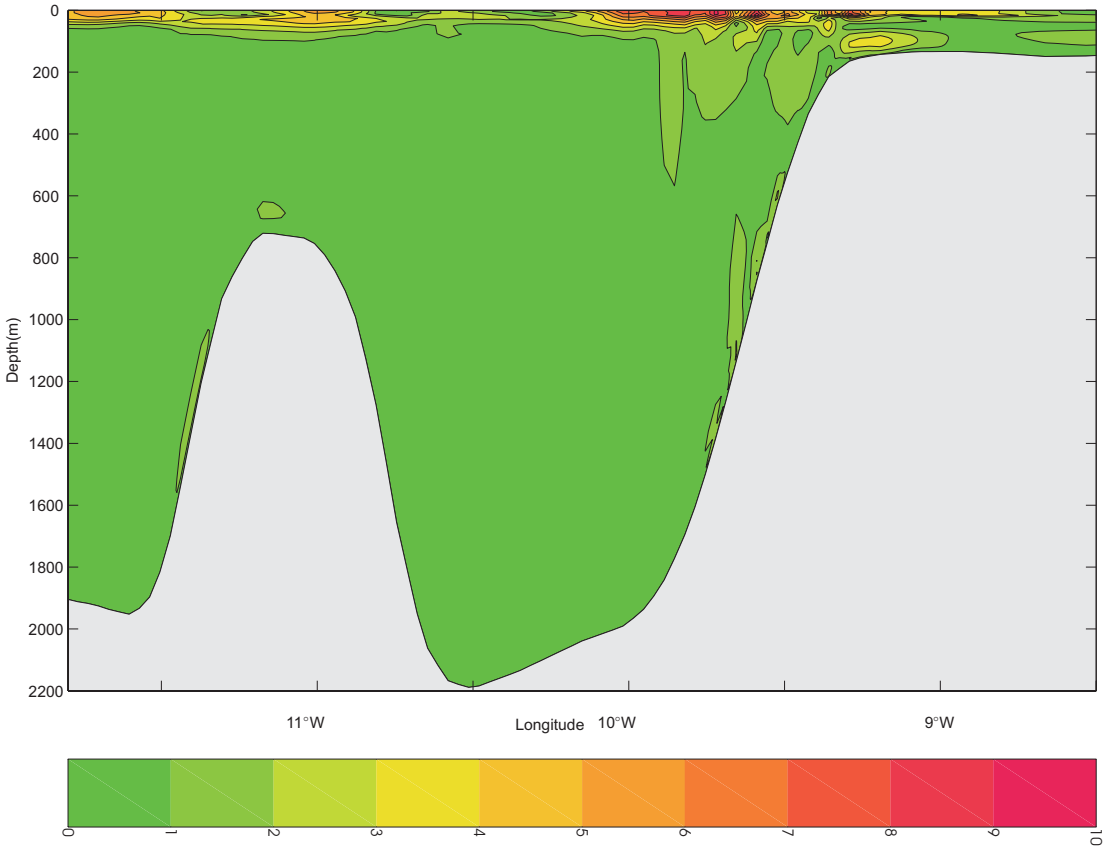

Fig. 12. Contours of the difference in baroclinic tidal amplitude (cm s^{-1}) between wind (0.2 Pa towards the South) and tidal solution and a tide only solution for short wind duration forcing (Calc. 4) at cross section D1n for the M_2 period.

wind induced mixing in the slope regions. As in HD05a, the model was forced with the M_2 barotropic tide. However, unlike in that paper where the emphasis was on the influence of grid resolution upon the M_2 tide and higher harmonics were not examined, here they are considered in detail. In essence the focus of the tide only calculations was an examination of the spatial distribution of the M_4 and M_6 internal tide. Calculations showed that with realistic topography and viscous effects there was no well defined point for the M_2 tide generation or well defined beams along which it propagated. This was rather different than the isolated seamount results of Lamb (2004) who showed narrow well defined beams for M_2 propagation with higher harmonics generated in regions where these beams intersected. This could give rise to mid–water generation of higher harmonics. The absence of narrow beams in the present calculations meant that higher harmonics were a maximum in the shelf slope region or on either side of the seamount, where the M_2 current and its horizontal derivative were a maximum. Similarly in the surface layer where the M_2 internal tide was reflected giving rise to local patches of internal tide current, with an associated horizontal gradient, regions of enhanced surface current amplitude at the higher harmonics occurred.

The absence of narrow beams of tidal energy in the present calculation is probably due to using realistic topography and including viscous and diffusive effects. As shown by Vlasenko et al. (2005), higher vertical modes are very rapidly damped when viscous and diffusive effects are included. This leads to appreciable broadening of the tidal beams, and a reduction of interaction between them. The application of realistic topography and an observed density profile means that there is no longer a single source of internal tide generation as would occur with constant buoyancy frequency and slope.

Calculated turbulence energy distributions and associated mixing, show that a region of cooler water occurs above the Anton Dohrn seamount. Such enhanced mixing above seamounts has been observed in a number of areas (e.g. Kunze and Toole 1997).

Short time scale calculations showed that the wind only modified the near surface stratification, and the change to the M_2 internal tidal current and its higher harmonics was restricted to the surface layer. Longer time scale calculations showed that both the tide and wind modified the temperature field at depth, giving rise to a modification of the density field and a change in the distribution of the internal tide and its harmonics.

On the short time scale changes in the M_2 internal tide and its higher harmonics produced with up–welling

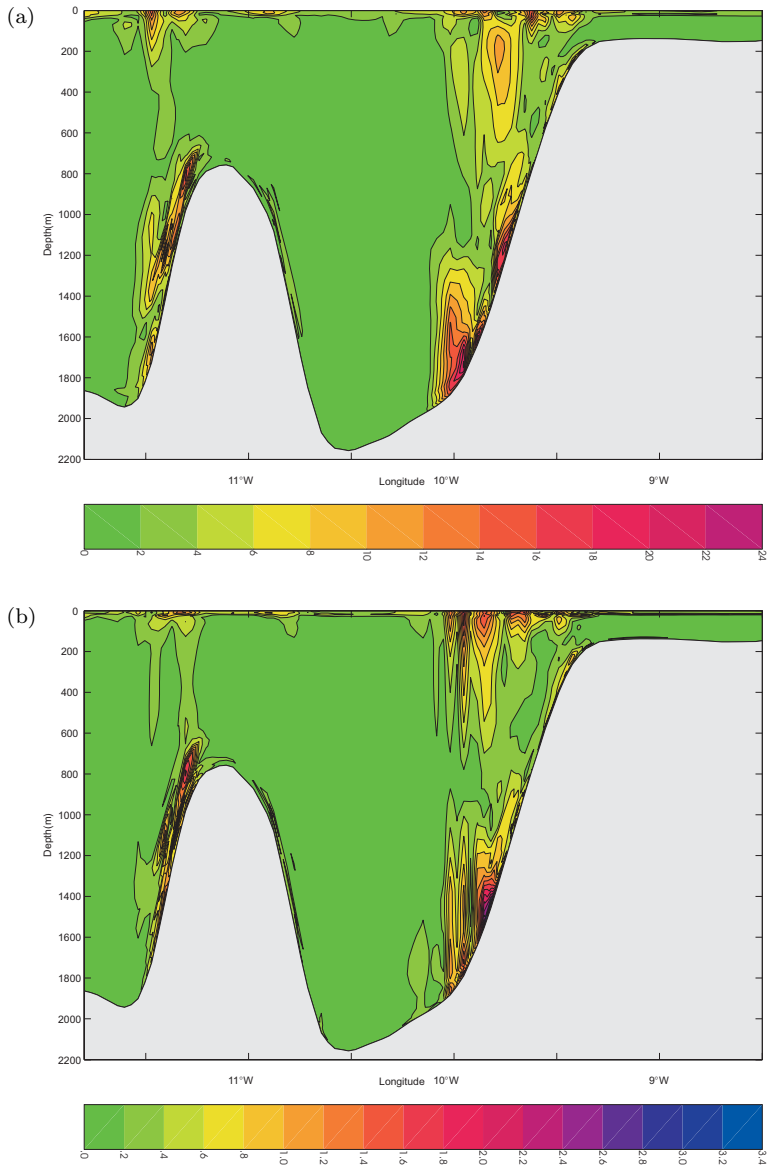

Fig. 13. As Fig. 9, but for a long duration wind (0.2 Pa towards the South) (Calc. 5), for (a) M_2, (b) M_4 and (c) M_6 frequency.

favourable winds were comparable to those found with the down–welling favourable wind. This similarity is because on the short time scale it is the mixing in the surface layer that has the greatest effect and this is not significantly influenced by wind direction. On the longer time scale there was more mixing in the slope regions, the extent of which depended on wind direction. Consequently the M_2 internal tide and its higher harmonics together with boundary layer turbulence and mixing were changed substantially more.

The calculations presented here clearly show that changes in the density field in regions of steep topography will have an impact upon the spatial distribution of the M_2 internal tide and its harmonics. In the present calculations these changes were produced by wind forcing. However along shelf flows of oceanic origin will also influence the density field in the region of internal tide generation. Effects such as this together with meteorological forcing will lead to significant variability of the M_2 internal tidal signal. Consequently non–linear interaction processes which give rise to higher harmonics and a cascade to turbulence and mixing will be affected. This has implications in terms of trying to partially validate these non–linear effects by seeing to what extent internal tidal models can reproduce the energy transfer to higher harmonics. In addition it impacts upon the spatial intensity required for data collection and model validation, using higher tidal harmonics. Similarly the small scale variability of turbulent kinetic energy, suggests that high spatial sampling is required to examine its distribution. Since its intensity is strongly related to the internal tide distribution in the bottom boundary layer, which depends on local topography and stratification these also need to be measured in detail. The fact that

the density field and hence the internal tide is modified by meteorological forcing suggests that it is important to obtain synoptic data sets for model validation. This is very different to the barotropic case where a comprehensive data set could be collected by sampling at different times.

ACKNOWLEDGEMENTS

The authors are indebted to Mrs L. Parry for typing the paper and Mr R.A. Smith for help in figure production. Access to bottom topography, open boundary forcing were provided by Dr J. Xing and are gratefully acknowledged. Access to the QUODDY code via the web site is much appreciated.

References

Berntsen, J., Xing, J., Davies, A. M., 2007. On the horizontal resolution required to resolve tidally forced internal waves and mixing at a sill with a numerical model. Submitted.

Blumberg, A. F., Mellor, G. L., 1987. A description of a three-dimensional coastal ocean circulation model. In: Heaps, N. S. (Ed.), Three-Dimensional Coastal Ocean Models. No. 4 in Coastal and Estuarine Sciences. American Geophysical Union, Washington, DC, p. 208pp.

Craig, P. D., 1987. Solutions for internal tide generation over coastal topography. Journal of Marine Research 45, 83–105.

Cummins, P. F., Oey, L. Y., 1997. Simulation of barotropic and baroclinic tides off Northern British Columbia. Journal of Physical Oceanography 27, 762–781.

Davies, A. M., Kwong, S. C. M., 2000. Tidal energy fluxes and dissipation on the European continental shelf. Journal of Geophysical Research 105, 21,969–21,989.

Davies, A. M., Lawrence, J., 1994. Modelling the non-linear interaction of wind and tide: its effect on current profiles. International Journal of Numerical Methods in Fluids 18, 163–188.

Flather, R. A., 1976. A tidal model of the north west European continental shelf. Memoires de la Societé Royale des Sciences de Liège 10, 141–164.

Fortunato, A. B., Baptista, A. M., Luettich, R. A., 1997. A three-dimensional model of tidal currents in the mouth of the Tagus estuary. Continental Shelf Research 17, 1689–1714.

Fortunato, A. B., Oliviera, A., Baptista, A. M., 1999. On the effect of tidal flats on the hydrodynamics of the Tagus estuary. Oceanologica Acta 22, 31–44.

Hall, P., Davies, A. M., 2005a. Comparison of finite difference and element models of internal tides on the Malin-Hebrides shelf. Ocean Dynamics 55, 272–293.

Hall, P., Davies, A. M., 2005b. Effect of coastal boundary resolution and mixing upon internal wave generation and propagation in coastal regions. Ocean Dynamics 55, 248–271.

Hall, P., Davies, A. M., 2005c. The influence of an irregular grid upon internal wave propagation. Ocean Modelling 10, 193–209.

Heniche, M., Secretin, Y., Boudreau, P., Leclerc, M., 2000. A two-dimensional finite element drying-wetting shallow water model for rivers and estuaries. Advances in Water Resources 23, 359–372.

Ip, J. T. C., Lynch, D. R., Friedrichs, C. T., 1998. Simulation of estuarine flooding and dewatering with application to Great Bay, New Hampshire. Estuarine, Coastal and Shelf Science 47, 119–141.

Jones, J. E., Davies, A. M., 2006. Application of a finite element model (TELEMAC) to computing the wind induced response of the Irish Sea. Continental Shelf Research 26, 1519–1541.

Jones, J. E., Davies, A. M., 2007. On the sensitivity of computed higher tidal harmonics to mesh size in a finite element model. Submitted.

Kunze, E., Toole, J. M., 1997. Tidally driven vorticity, diurnal shear, and turbulence atop Fieberling Seamount. Journal of Physical Oceanography 27, 2663–2693.

Lamb, K. G., 2004. Non-linear interaction among internal wave beams generated by tidal flow over supercritical topography. Geophysical Research Letters 31, L09313.

Luyten, P. J., Deleersnijder, E., Ozer, J., Ruddick, K. G., 1996. Presentation of a family of turbulence closure models for stratified shallow water flows and preliminary application to the Rhine outflow region. Continental Shelf Research 16, 101–130.

Proctor, R., James, I. D., 1996. A fine-resolution 3D model of the southern North Sea. Journal of Marine Systems 8, 285–295.

Samelson, R. M., 1998. Large scale circulation with locally enhanced vertical mixing. Journal of Physical Oceanography 28, 712–726.

Sherwin, T. J., Taylor, N. K., 1989. The application of a finite difference model of internal tide generation to the NW European Shelf. Deutsche Hydrographische Zeitschrift 42, 151–167.

Sherwin, T. J., Taylor, N. K., 1990. Numerical investigations of linear internal tide generation in the Rockall Trough. Deep-Sea Research 37, 1595–1618.

Smagorinsky, J., 1963. General circulation experiments with the primitive equations I. The basic experiment. Monthly Weather Review 91, 99–164.

Spall, M. A., 2001. Large scale circulations forced by localized mixing over a sloping bottom. Journal of Physical Oceanography 31, 2369–2384.

Vlasenko, V., Stashchuk, N., Hutter, K., 2005. Baroclinic tides: Theoretical modeling and observational evidence. Cambridge University Press, Cambridge, UK.

Walters, R. A., 2005. Coastal ocean models: two useful finite element methods. Continental Shelf Research 25, 775–794.

Walters, R. A., Werner, F. E., 1989. A comparison of two finite element models of tidal hydrodynamics using a North Sea data set. Advances in Water Resources 12,

184–193.

Werner, F. E., 1995. A field test case for tidally forced flows: a review of the tidal flow forum. In: Lynch, D. R., Davies, A. M. (Eds.), Quantitative Skill Assessment for Coastal Ocean Models. American Geophysical Union, Washington, DC, pp. 269–284.

Xing, J., Davies, A. M., 1996a. Application of turbulence energy models to the computation of tidal currents and mixing intensities in shelf edge regions. Journal of Physical Oceanography 26, 417–447.

Xing, J., Davies, A. M., 1996b. Processes influencing the internal tide, its higher harmonics, and tidally induced mixing on the Malin-Hebrides shelf. Progress in Oceanography 38, 155–204.

Xing, J., Davies, A. M., 1997. The influence of wind effects upon internal tides in shelf edge regions. Journal of Physical Oceanography 27, 205–262.

Xing, J., Davies, A. M., 1998. A three-dimensional model of internal tides on the Malin-Hebrides shelf and shelf edge. Journal of Geophysical Research 103(C) (12), 27821–27847.

Xing, J., Davies, A. M., 1999. The influence of topographic features and density variations upon the internal tides in shelf edge regions. International Journal of Numerical Methods in Fluids 31, 535–577.